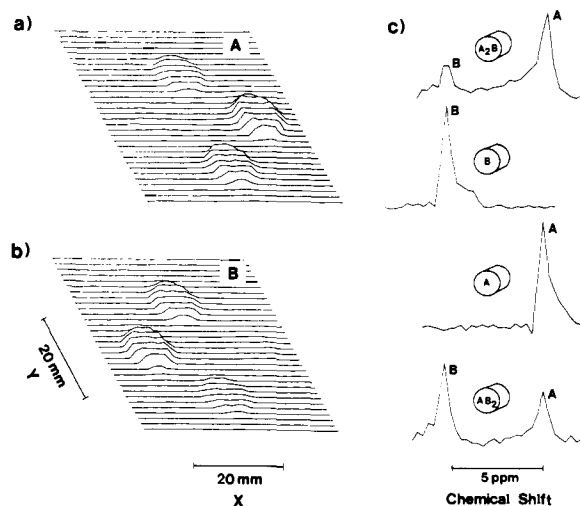


**Figure 3.** (a) Representative echo-train signal observed by applying the pulse sequence shown in Figure 2. Note that (i) each echo shape is governed by the field gradient  $G_X$ , yielding the spatial information, and (ii) the echo envelope corresponds to the normal free induction decay giving the high-resolution spectrum. (b) Rearrangement of echo trains. Odd- and even-numbered echoes are separately rearranged to give two sets of two-dimensional arrays, in which the time axis  $t_s$  corresponds to the spectral axis and the time axis  $t_x$  to the spatial axis  $X$ .

be reduced by one in comparison with the usual multidimensional FT method.<sup>3</sup>

Experiments were performed at 0.5 T, operating our NMR imager<sup>9</sup> for protons. Figure 1 shows our two-dimensional test sample consisting of acetone (A) and benzene (B); the proton chemical-shift difference is 5.1 ppm. The pulse sequence used for the measurement is schematically shown in Figure 2. If a periodically inverting magnetic field gradient  $G_X$  is imposed on a sample during observation of a free induction decay, the resultant signal takes the form of a spin-echo train as shown in Figure 3a. Such an echo-train signal is modulated by both internal magnetic interactions within the sample, which give high-resolution spectra, and an external interaction generated by the time-dependent field gradient, which provides one-dimensional spatial information  $X$ . Consequently, the two distinct types of information can be extracted from the single echo train.<sup>6,8</sup> Furthermore, remaining spatial information  $Y$  can be phase encoded<sup>5</sup> into the echo-train signal by pulsed applications of a field gradient  $G_Y$ . In each phase-encoded (or phase-modulated) echo train, odd- and even-numbered echoes are separately rearranged to give two sets of two-dimensional arrays as shown in Figure 3b;<sup>8a</sup> along the new time axis  $t_s$ , one can observe free induction decays which give high-resolution spectra, because the effects of the external interaction on the signals are quenched along the new time axis.<sup>10</sup> The echo shapes are governed by the external interaction ( $G_X$ ), which is represented on the  $t_x$  axis (Figure 3b). Since the spatial information  $Y$  is already phase-encoded along the third axis  $t_Y$  perpendicular to both array axes  $t_s$  and  $t_x$ , three-dimensional Fourier transformation of either set of the three-dimensional rearranged data ( $t_s, t_x, t_Y$ ) can yield chemically resolved proton images and spatially resolved proton high-resolution spectra as



**Figure 4.** Proton images of acetone (a) and benzene (b), and proton high-resolution spectra at four different locations (c). Two echo trains were added in each step of 32 phase encodings with a repetition time 500 ms, the total measurement time being only 32 s. Both the  $X$  and  $Y$  axes are represented by 32 points and the spectra by 32 points, interpolated from 16 points using the zero-filling technique; the number of spectral data points is limited by the memory size of our signal averager (1024 points). The images were obtained from the spectral intensities of absolute values of the Fourier transforms while the local spectra are of phase-corrected absorption mode. The use of absolute values can solve a dephasing problem caused by homonuclear  $J$  couplings. Each local spectrum shifts depending upon the field strength at the corresponding location with the spectral separation preserved. The spectral resolution of each local spectrum is limited by the corresponding local field inhomogeneity,<sup>11</sup> as in the multidimensional FT method.<sup>3b,c</sup>

shown in Figure 4. It should be noted that the two sets of three-dimensional FT data can mutually be coadded after correcting the sign difference in  $X$ .<sup>6a,b</sup> For three-dimensional objects, another phase encoding and Fourier transformation are necessary along the  $Z$  direction.

**Acknowledgment.** We thank Hidemi Shiono for his skillful help in assembling a signal-acquisition program.

### Kinetic Isotope Effect in Gas-Phase Base-Induced Elimination Reactions

Veronica M. Bierbaum,\* Jonathan Filley, and Charles H. DePuy

Department of Chemistry, University of Colorado  
Boulder, Colorado 80309

Martin F. Jarrold and Michael T. Bowers\*

Department of Chemistry, University of California  
Santa Barbara, California 93106

Received December 5, 1984

Most exothermic gas-phase ion-molecule reactions are rapid, occurring at essentially every collision. This arises because long-range electrostatic forces exist between the ion and neutral; these species, therefore, attract one another and interact with sufficient energy to surmount many traditional barriers to reaction. Nevertheless, there is increasing evidence that these processes can be highly specific. We wish to report the observation of a dramatic example of reaction selectivity: a hydrogen/deuterium isotope effect of 5.5, which is close to the theoretical maximum, in the elimination reaction of amide ion with diethyl ether. Modeling both the absolute rate and isotope effect using statistical rate theory provides insight to the barrier height and reaction mechanism for this process.

(9) (a) Matsui, S.; Yamamoto, E.; Kuroda, M.; Shiono, H.; Kohno, H.; Ohtomo, H.; Kato, H.; Kogure, K., Proceedings of the 22nd NMR symposium in Japan, Kyoto, Japan, Nov 1983. (b) Kato, H.; Kogure, K.; Ohtomo, H.; Tobita, M.; Matsui, S.; Yamamoto, E.; Kohno, H. *J. Cereb. Blood Flow Metab.*, in press.

(10) To realize this quenching experimentally, precise timing adjustment was made for the inversions of the field gradient  $G_X$  so that the field-gradient effect on spin phases is always cancelled at times  $2\tau_e + 2N\tau$  ( $N = 0, 1, 2, 3, \dots, 31$ ) (see Figure 2).

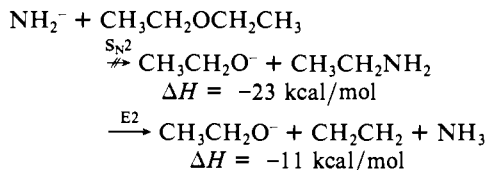
(11) It may be worth noting that if the object is in fact spatially homogeneous, all the local spectra can be coadded after correcting the spectral shifts; therefore, spectral broadening due to overall field inhomogeneity is avoidable even if the sample is very large.

Table I

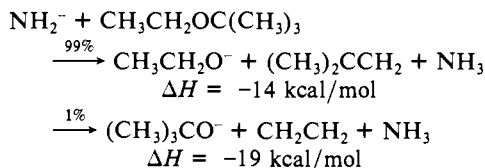
reaction	$k_{\text{exptl}}^a$	reaction efficiency <sup>b</sup>		$\Delta E^c$ kcal/mol
		exptl	theory	
$\text{NH}_2^- + \text{CH}_3\text{CH}_2\text{OCH}_2\text{CH}_3$	4.4	0.19	0.18 <sup>d</sup>	1.6 <sup>d</sup>
$\text{NH}_2^- + \text{CD}_3\text{CD}_2\text{OCD}_2\text{CD}_3$	0.8	0.035	0.038 <sup>d</sup>	0.5 <sup>d</sup>
$\text{HO}^- + \text{CH}_3\text{CH}_2\text{OCH}_2\text{CH}_3$	5.8	0.26	0.26	4.6
$\text{HO}^- + \text{CD}_3\text{CD}_2\text{OCD}_2\text{CD}_3$	2.7	0.12	0.12	3.5

<sup>a</sup>Units of  $10^{-10} \text{ cm}^3 \text{ molecule}^{-1} \text{ s}^{-1}$ . <sup>b</sup> $k_{\text{reaction}}/k_{\text{collision}}$ . <sup>c</sup> $\Delta E$  is the difference between the zero point energy of the reactants and the zero point energy of the transition state. The reaction coordinate was assumed to be a C-H or C-D bond. The difference in barrier heights in the protio and deuterio systems ( $\Delta E_{\text{H}} - \Delta E_{\text{D}}$ ) is simply the difference in zero point energies of the C-H and C-D bonds ( $1/2 h\nu_{\text{CH}} - 1/2 h\nu_{\text{CD}} = 1.1 \text{ kcal/mol}$ ). <sup>d</sup>Essentially equivalent reaction efficiencies were obtained for  $\Delta E$  values of 2.3 (protio) and 1.2 kcal/mol (deuterio) with somewhat different frequencies of the newly formed transitional modes in the transition state. These differences reflect the uncertainty in the barrier heights determined using the phase space modeling methods.

We have previously reported<sup>1</sup> that the gas-phase reactions of strong bases with ethers exhibit reaction specificity on two levels. First there is selection between reaction channels that represent different mechanisms. For example, in the reaction of amide with diethyl ether, although both nucleophilic substitution and elimination reactions are exothermic, elimination is observed exclusively.<sup>2</sup>



Second, there is selection between mechanistically similar channels. In the reaction of amide with ethyl *tert*-butyl ether there is strong preference for production of ethoxide ion rather than *tert*-butoxide, although the thermochemistry of the two elimination pathways is similar.



Recently we have observed high reaction specificity in these systems on a third level, selection between channels that differ only by isotope substitution. Using a flowing afterglow apparatus,<sup>3</sup> we have measured the rate constants for reactions of amide and hydroxide ions with diethyl ether and diethyl-*d*<sub>10</sub> ether. These results are summarized in Table I.<sup>4</sup> Reaction occurs on one in every four or five collisions<sup>5</sup> for the undeuterated ether; however, introduction of deuterium decreases the reaction rate by factors of 5.5 for amide and 2.1 for hydroxide. Although isotope effects in gas-phase ion-molecule reactions have been observed by other workers,<sup>6</sup> the magnitude of the effect in the ether system is un-

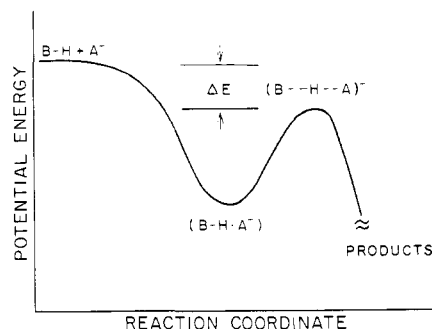


Figure 1. Schematic reaction coordinate diagram for the elimination reactions in Table I. A similar diagram pertains to the D-abstraction process.

usually large. We have observed similar isotope effects in the reactions of  $\text{NH}_2^-$  and  $\text{HO}^-$  with  $\text{CH}_3\text{CH}_2\text{OCD}_2\text{CD}_3$  in which  $\text{CD}_3\text{CD}_2\text{O}^-$  is the major product. Therefore, the preferential attack at C-H rather than C-D bonds is both an intermolecular and intramolecular phenomenon. Neither amide nor hydroxide ion shows a detectable secondary isotope effect since their reactions with  $\text{CH}_3\text{CD}_2\text{OCH}_2\text{CH}_3$  produce equal amounts of  $\text{CH}_3\text{CD}_2\text{O}^-$  and  $\text{CH}_3\text{CH}_2\text{O}^-$ .

We have modeled these data using statistical rate theory.<sup>7</sup> A schematic reaction coordinate diagram is given in Figure 1. All vibrational frequencies and rotational constants, except for the transition state, were taken from the literature.<sup>8</sup> We were able to obtain an excellent fit of the data using a model in which the C-H or C-D symmetric stretch is chosen as the reaction coordinate but in which other bonds have not changed in the transition state<sup>9</sup> (i.e., an  $\text{E}1_{\text{cb}}$ -like mechanism<sup>10</sup>). The barrier height and transition-state frequencies are two independent, strongly varying functions and simultaneously fitting both the isotope effect and absolute rate provides a fairly stringent set of limits. The results of this analysis indicate that the transition states for reactions of amide and hydroxide ions with diethyl ether lie only about 2 and 5 kcal, respectively, below the energy of the reactants (see Table I).<sup>11</sup> Thus, despite the large attractive forces in these ion-molecule systems and the large reaction rates, the presence of substantial barriers along the reaction coordinate can induce strikingly specific

(7) Chesnavich, W. J.; Bowers, M. T. *J. Am. Chem. Soc.* **1976**, *98*, 8301. Chesnavich, W. J.; Bass, L.; Su, T.; Bowers, M. T. *J. Chem. Phys.* **1981**, *74*, 2228-2246. Bowers, M. T.; Jarrold, M. F.; Wagner-Redeker, W.; Kemper, P. R.; Bass, L. *Faraday Discuss. Chem. Soc.* **1983**, *75*, 57-76.

(8) The vibrational frequencies and rotational constants for  $\text{NH}_2^-$  were assumed to be identical with those for  $\text{NH}_2$  (Herzberg, G. "Molecular Spectra and Molecular Structure III—Electronic Spectra and Electronic Structure of Polyatomic Molecules"; D. Van Nostrand Co.: Princeton, NJ, 1967) since the photoelectron spectrum of  $\text{NH}_2^-$  shows a single peak (Celotta, R. J.; Bennett, R. A.; Hall, J. L. *J. Chem. Phys.* **1974**, *60*, 1740-1745). The vibrational frequency and rotational constant for  $\text{HO}^-$  were taken from Huber and Herzberg (Huber, K. P.; Herzberg, G. "Constants of Diatomic Molecules"; Van Nostrand Reinhold Co., New York, 1979). Vibrational frequencies for  $\text{C}_4\text{H}_{10}\text{O}$  and  $\text{C}_4\text{D}_{10}\text{O}$  were taken from Wieser et al. (Wieser, H.; Laidlaw, W. G.; Krueger, P. J.; Fuhrer, H., *Spectrochim. Acta, Part A* **1968**, *24A*, 1055-1089). Rotational constants for  $\text{C}_4\text{H}_{10}\text{O}$  were taken from Hayashi and Kuwada (Hayashi, M.; Kuwada, K. *Bull. Chem. Soc. Jpn.* **1974**, *47*, 3006-3009); rotational constants for  $\text{C}_4\text{D}_{10}\text{O}$  were calculated from the atomic masses and coordinates. The molecular polarizability of  $\text{C}_4\text{H}_{10}\text{O}$  was taken from Miller and Savchik (Miller, K. J.; Savchik, J. A. *J. Am. Chem. Soc.* **1979**, *101*, 7206-7213).

(9) This model of a symmetrical transition state for reactions of both  $\text{NH}_2^-$  and  $\text{HO}^-$  allows an excellent fit of the isotope effect and absolute rate constants. Additional experiments and calculations will test the usefulness of more complex models, such as those utilized to describe isotope effects on  $\text{E}2$  reactions in solution. According to this picture, the greater isotope effect of the more exothermic amide-induced elimination indicates an earlier and hence a more central transition state for  $\text{HO}^-$  (see: Lowry, T. H.; Richardson, K. S. "Mechanism and Theory in Organic Chemistry", 2nd ed.; Harper and Row: New York, 1981; pp 197-210).

(10) Saunders, W. H., Jr.; Cockerill, A. F. "Mechanisms of Elimination Reactions"; Wiley: New York, 1973.

(11) Pellerite and Brauman have shown that the  $\text{S}_{\text{N}}2$  transition state for an ether lies above the energy of the reactants and indeed dimethyl ether does not react with either  $\text{NH}_2^-$  or  $\text{HO}^-$  in the gas phase. Pellerite, M. J.; Brauman, J. I. *J. Am. Chem. Soc.* **1980**, *102*, 5993-5999.

(1) DePuy, C. H.; Bierbaum, V. M. *J. Am. Chem. Soc.* **1981**, *103*, 5034-5038.

(2) Proton abstraction is presumably endothermic. For the reaction of hydroxide ion with diethyl ether the elimination reaction is allowed by entropy ( $\Delta H = +2 \text{ kcal/mol}$ ;  $\Delta G = -9 \text{ kcal/mol}$ ).

(3) DePuy, C. H.; Bierbaum, V. M. *Acc. Chem. Res.* **1981**, *14*, 146-153.

(4) Isotope exchange in the reactant bases is not observed; this indicates that the initial proton transfer is not reversible.

(5) Su, T.; Bowers, M. T. *Int. J. Mass Spectrom. Ion Phys.* **1973**, *12*, 347-356.

(6) See, for example: Wellman, K. M.; Victoriano, M. F.; Isolani, P. C.; Riveros, J. M. *J. Am. Chem. Soc.* **1979**, *101*, 2242-2243. Klass, G.; Underwood, D. J.; Bowie, J. H. *Aust. J. Chem.* **1981**, *34*, 507-517. Noest, A. J.; Nibbering, N. M. M. *Int. J. Mass Spectrom. Ion Phys.* **1980**, *34*, 383-385.

chemistry. We hope that the combination of experimental isotope effects with the appropriate theoretical analysis will prove to be as revealing about the mechanisms of gas-phase ion-molecule reactions as they have about reactions in solution.

**Acknowledgment.** We gratefully acknowledge support of this research by the National Science Foundation under Grants CHE82-03110 (V.M.B. and C.H.D.) and CHE80-20464 (M.T.B.).

**Registry No.** CH<sub>3</sub>CH<sub>2</sub>OCH<sub>2</sub>CH<sub>3</sub>, 60-29-7; NH<sub>2</sub><sup>-</sup>, 17655-31-1; HO<sup>-</sup>, 14280-30-9; deuterium, 7782-39-0.

### Assignment of Complex <sup>1</sup>H NMR Spectra via Two-Dimensional Homonuclear Hartmann-Hahn Spectroscopy

Donald G. Davis and Ad Bax\*

Laboratory of Chemical Physics  
National Institute of Arthritis, Diabetes  
and Digestive and Kidney Diseases  
National Institutes of Health  
Bethesda, Maryland 20205

Received January 15, 1985

We propose the use of a new type of two-dimensional NMR experiment for the determination of homonuclear scalar connectivity in complex molecules. The method relies on the principle of cross polarization, first introduced by Hartmann and Hahn<sup>1</sup> and commonly used for sensitivity enhancement in solid-state <sup>13</sup>C NMR.<sup>2</sup> In our experiment homonuclear cross polarization is obtained by switching on a single coherent rf field. In cases where the effective rf field strengths experienced by two scalar coupled protons are identical, a perfect Hartmann-Hahn match is established and gives rise to oscillatory exchange (with period 1/*J*) of spin-locked magnetization. For a simple two-spin AX system complete exchange of magnetization is obtained for a spin-lock time equal to 1/(2*J*<sub>AX</sub>). For larger spin systems the time dependence of the magnetization exchange follows a more complicated pattern (to be published). Two pulse schemes relying on homonuclear cross polarization are sketched in Figure 1. In Figure 1a a coherent rf field of constant phase is switched on for a mixing time of duration τ<sub>m</sub>. The projection of the vector sum of all magnetization components of the multiplet of an arbitrary spin, A, will be spin locked along the rf field, whereas most of the magnetization perpendicular to the spin-lock field will dephase rapidly due to spatial inhomogeneity of the rf field. For a proton, A, with offset Δ<sub>A</sub> from the carrier frequency, the effective rf field strength, ν<sub>A</sub>, is to a good approximation given by

$$\nu_A = \nu + \Delta_A^2/2\nu \quad (1)$$

provided that the nominal rf field strength ν ≫ Δ<sub>A</sub>. Analogous to expressions derived by Müller and Ernst<sup>3</sup> and Chingas et al.<sup>4</sup> for the heteronuclear case, it can be shown that effective magnetization transfer between protons A and X is possible if

$$|\Delta_A^2 - \Delta_X^2|/2\nu < |J_{AX}| \quad (2)$$

at a rate that depends on *J*<sub>AX</sub> and on |ν<sub>A</sub> - ν<sub>X</sub>|.<sup>3,4</sup> From eq 1 it follows that large rf field strengths, ν, are generally required for effective transfer. Alternatively, this condition can be fruitfully used to restrict magnetization transfer to distinct regions of the spectrum. For example, magnetization transfer between amide and C<sub>α</sub> protons in peptides can be obtained by positioning the

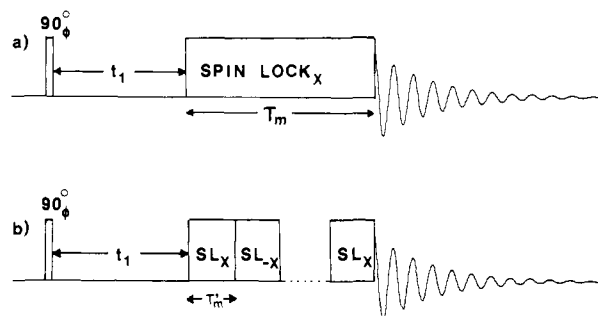


**Figure 1.** Pulse schemes for 2D homonuclear cross polarization (a) without compensation for different effective field strengths and (b) with compensation. The phase, φ, of the 90° <sup>1</sup>H pulse is cycled along all four axes, and data for odd- and even-numbered scans are stored in separate locations to allow a hypercomplex 2D Fourier transformation.<sup>3</sup>

carrier frequency midway between the amide and α spectral regions. Restrictions imposed by eq 2 on the bandwidth that can be covered by the new method can be alleviated by alternating the phase of the applied rf field along the ±*x* axis at a rate 1/τ<sub>m</sub>. To prevent rotary echo effects,<sup>5</sup> the total durations that the rf field is applied along the *x* and -*x* axis are made different (Figure 1b). It can be shown that effective magnetization transfer, at a rate determined by *J*<sub>AX</sub>, is now possible under the condition

$$\tau_m' |\Delta_A^2 - \Delta_X^2|/2\nu < 0.25 \quad (3)$$

A major advantage of homonuclear cross polarization is that net magnetization transfer occurs and a phase sensitive 2D spectrum with all peaks in the near absorption mode can be obtained. This is in contrast with the COSY experiment<sup>6-9</sup> where diagonal and cross peaks are 90° out of phase and individual cross multiplet components are 180° out of phase relative to one another, causing partial signal cancellation and sensitivity loss. In our new experiment there is also some dispersive character to the individual diagonal and cross multiplets.<sup>3,4,10</sup> However, their antiphase nature causes significant mutual cancellation while the absorptive components remain, and therefore the spectrum appears to be in the absorption mode. Another consequence of the net magnetization transfer is the introduction of relayed connectivity; magnetization that is transferred from proton A to proton M during the first half of the mixing period will be relayed in part to proton X during the second half of the mixing period, provided that *J*<sub>AM</sub> and *J*<sub>MX</sub> are not zero. For short mixing periods (<20 ms) little relay will be observed, but for longer mixing times single-relay and multiple-relay effects become significant.

As an example, the method is demonstrated for a sample of 1 mg of alamethicin, dissolved in 0.4 mL of methanol-*d*<sub>4</sub>. Alamethicin is an icosapeptide with the sequence Ac-Aib-Pro-Aib-Ala-Aib-Ala-Gln-Aib-Val-Gly-Leu-Aib-Pro-Val-Aib-Aib-Glu-Gln-Phol. The alamethicin was kindly provided by Dr. G. B. Whitfield of the Upjohn Co. and purified as described by Gisin et al.<sup>11</sup> Experiments were carried out on a Nicolet 500-MHz spectrometer, using a mixing time of 7 × 5 ms, i.e., four periods of 5 ms spin locked along the *x* axis interleaved with three periods along the -*x* axis. 5-W rf power was used to generate a 10-kHz rf field. Figure 2a shows the regular 1D spectrum of the aliphatic region and Figure 2b shows the 2D spectrum obtained with the new method, not treated by symmetrization<sup>12</sup> or other white-wash procedures. Connectivities observed in this spectrum basically

(5) Solomon, I. *Phys. Rev. Lett.* **1959**, *2*, 301.

(6) Aue, W. P.; Bartholdi, E.; Ernst, R. R. *J. Chem. Phys.* **1976**, *64*, 2229.

(7) Bax, A.; Freeman, R. *J. Magn. Reson.* **1981**, *44*, 542.

(8) Nagayama, K.; Kumar, A.; Würthrich, K.; Ernst, R. R. *J. Magn. Reson.* **1980**, *40*, 321.

(9) Marion, D.; Würthrich, K. *Biochem. Biophys. Res. Commun.* **1984**, *56*, 207.

(10) Braunschweiler, L.; Ernst, R. R. *J. Magn. Reson.* **1983**, *53*, 521.

(11) Gisin, B. F.; Davis, D. G.; Borowska, Z. K.; Hall, J. E.; Kobayashi, S. *J. Am. Chem. Soc.* **1981**, *103*, 6373.

(1) Hartmann, S. R.; Hahn, E. L. *Phys. Rev.* **1962**, *128*, 2042.  
(2) Pines, A.; Gibby, M. G.; Waugh, J. S. *J. Chem. Phys.* **1973**, *59*, 569.  
(3) Müller, L.; Ernst, R. R. *Mol. Phys.* **1980**, *38*, 963.  
(4) Chingas, G. C.; Garroway, A. N.; Bertrand, R. D.; Moniz, W. B. *J. Chem. Phys.* **1981**, *74*, 127.